

Theoretical Analysis of the Inter-Ligand Overhauser Effect: A New Approach for Mapping Structural Relationships of Macromolecular Ligands

Robert E. London

Laboratory of Structural Biology, MR-01, NIEHS, Box 12233, Research Triangle Park, North Carolina 27709

Received April 26, 1999; revised July 29, 1999

A theoretical framework has been developed for the evaluation of inter-ligand Overhauser effects (ILOE), predicted when pairs of ligands are observed in the presence of a macromolecular receptor which can form a ternary complex such that some of the protons on the two ligands are in close proximity with each other (generally less than $\sim 5 \text{ \AA}$). Simulations for a pair of ligands with three spins each have been performed for a variety of geometric and rate parameters. Analogous to previously described calculations of TRNOE behavior, theoretical behavior of each of the nine cross peaks, A_{ij} , in a NOESY experiment involving ligands which can exist in the free, binary, or ternary complex states can be calculated. However, for exchange which is sufficiently rapid on the relaxation and chemical shift time scales, use of a collapsed matrix, C , corresponding to sums of sets of nine elements, will often be appropriate and generally simplifies the analysis. In order to generate inter-ligand Overhauser effects, it is optimal for the fraction of receptor involved in the ternary complex to be reasonably large; i.e., concentrations of both ligands should be near saturation. Based on a model assuming random binding order of the ligands, the dependence of ILOE resonance intensities on kinetic rate constants roughly parallels the dependence of transferred NOE (TRNOE) intensities. For diffusion controlled binding, i.e., $k_{on} \sim 10^8 \text{ M}^{-1} \text{ s}^{-1}$, the method is best suited for equilibrium dissociation constants in the micromolar–millimolar range ($k_{off} \sim 10^2\text{--}10^5 \text{ s}^{-1}$). Toward the slower dissociation rate constant end of this range, TRNOE and ILOE effects are still predicted, but the initial build-up curves become markedly nonlinear. For a kinetic binding scheme which assumes ordered binding of the ligands, the inherent asymmetry of the ligand binding process leads to more complex kinetics and alters the dependence of the ILOE on the kinetic parameters. In this case, the binding of the second ligand effectively reduces the exchange rate of the first ligand, reducing the transfer of NOE and ILOE information. The reduction in TRNOE and ILOE information which is predicted for the ordered ligand binding model is overcome at larger dissociation rate constants for either ligand 1 or ligand 2. In addition to the structural information available from ILOE data, the strong dependence of TRNOE and ILOE curves on ordered ligand binding suggests that such measurements could be useful for the characterization of ligand binding kinetics.

INTRODUCTION

Enzymes catalyze bimolecular reactions by bringing pairs of reactants together and creating an environment which facilitates the reaction. When pairs of substrates or substrate–cofactor combinations are complexed in the active site of an enzyme, some of the nuclei on the two ligands may be sufficiently close to interact magnetically, leading to a perturbation of the NMR relaxation parameters and to an inter-ligand nuclear Overhauser effect. In order to evaluate the transfer of this interaction to the pair of free ligands, we have extended the formalism previously developed to describe the transferred NOE (I) to include two reversibly bound ligands. These calculations support the existence of such an effect, and provide insight into the dependence on kinetic and geometric parameters. Thus, there can be a transfer of the inter-ligand Overhauser effect (ILOE) present in the complex to the pair of uncomplexed ligands, which are able to store the NOE information due to the slower spin–lattice relaxation in the more highly mobile, uncomplexed state. This type of effect has many potential applications including determination of the structure of active site complexes involved in enzyme catalysis. Additionally, one may envision extension to the analysis of ligands not directly related to substrates, and hence to the development of enzyme inhibitors. We have recently been able to verify these predictions experimentally (2).

THEORY

The time development of the cross peak intensities in a NOESY experiment can be described by a differential equation according to the relation (3–6)

$$\frac{d\mathbf{A}}{dt} = -\mathbf{R}\mathbf{A}, \quad [1]$$

where \mathbf{A} represents the matrix of cross peak intensities and \mathbf{R} is the relaxation matrix with diagonal elements

$$R_{ii} = \sum_j \rho_{ij} + \rho_i^* \quad [2]$$

with the dipolar contributions to the spin–lattice relaxation rate ρ_{ij} given by

$$\rho_{ij} = \frac{\gamma_i^2 \gamma_j^2 \hbar^2}{10r_{ij}^6} [J_0(\omega) + 3J_1(\omega) + 6J_2(\omega)] \quad [3]$$

and off diagonal elements

$$R_{ij} = \sigma_{ij} = \frac{\gamma_i^2 \gamma_j^2 \hbar^2}{10r_{ij}^6} [6J_2(\omega) - J_0(\omega)] \quad [4]$$

with the spectral densities defined by

$$J_n(\omega) = \frac{\tau_{ij}}{1 + (n\omega_0\tau_{ij})^2} \quad [5]$$

In the above, τ_{ij} is the (isotropic) rotational correlation time for the internuclear vector between nuclei i and j and ω_0 is the Larmor frequency. Cross-correlation terms between interactions leading to relaxation are neglected in the above treatment. The leakage term ρ^* is generally set equal to 1 s^{-1} , and arises due to mobile portions of the protein which more effectively couple the magnetization to the lattice (7). In practice, it is convenient to calculate the relaxation matrix using a similarly sized interproton distance matrix, as described by Khan *et al.* (8), with elements $D_{ij} = r_{ij}$. Equation [1] may be formally solved for a given mixing time t_m to yield

$$\mathbf{A}(\tau_m) = \chi \cdot \exp(-\lambda t_m) \cdot \chi^{-1} \cdot \mathbf{A}(0), \quad [6]$$

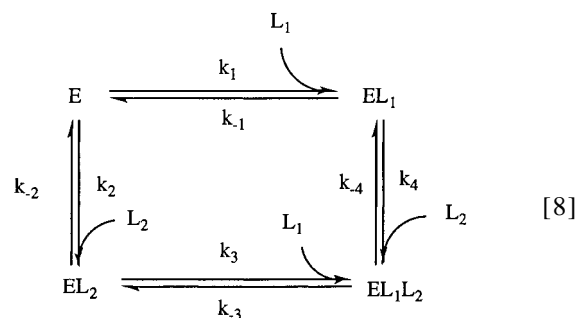
where χ is the matrix of eigenvectors for the relaxation matrix \mathbf{R} , λ is the diagonal matrix of eigenvalues (6), and $\mathbf{A}(0)$ is the initial value matrix, discussed below.

In order to evaluate the conditions under which inter-ligand Overhauser effects (ILOEs) can be observed, we have generalized our previous relaxation matrix treatment describing a single, reversibly bound ligand (1) to cover the case of a pair of ligands which can form either a binary or ternary complex with a receptor. For the ILOE calculation, the relaxation matrix is expanded to describe the free ligands L_1 and L_2 , the two binary complexes, EL_1 and EL_2 , and finally the ternary complex, EL_1L_2 , where we have used the symbol “E” for the receptor to avoid confusion with the symbol for the relaxation matrix. We thus obtain an expanded relaxation matrix of the form:

$$\mathbf{R}' = \begin{array}{c} \begin{array}{ccccc} & n & & m & & n & & m & & n+m \\ \hline \mathbf{R}(L_1, \tau_{1F}) & & & & & & & & & & \\ \hline & & \mathbf{R}(L_2, \tau_{2F}) & & & & & & & & \\ \hline & & & & \mathbf{R}(L_1, \tau_B) & & & & & & \\ \hline & & & & & & & \mathbf{R}(L_2, \tau_B) & & & \\ \hline & & & & & & & & & \mathbf{R}(L_1L_2, \tau_B) & \\ \hline \end{array} & \begin{array}{l} n \\ m \\ n \\ m \\ n+m \end{array} \end{array} \quad [7]$$

where $\mathbf{R}(L_1, \tau_{1F})$ is the relaxation matrix calculated as described above by Eqs. [2]–[5] for ligand 1 in the free state, whose motion corresponds to a rotational correlation time τ_{1F} . $\mathbf{R}(L_2, \tau_{2F})$ is the corresponding relaxation matrix for ligand 2 in the uncomplexed state; $\mathbf{R}(L_1, \tau_B)$ corresponds to ligand 1 in the binary complex with the receptor, with rotational correlation time τ_B . $\mathbf{R}(L_2, \tau_B)$ is the corresponding relaxation matrix for L_2 in the binary complex. Finally, $\mathbf{R}(L_1L_2, \tau_B)$ is the relaxation matrix for the ternary complex. The dimensions of the submatrices, indicated above, correspond to the n spins in ligand 1 and m spins in ligand 2. Thus, the first and third relaxation submatrices above have dimensions $n \times n$, the second and fourth have dimensions $m \times m$, and the ternary complex matrix has dimensions $n + m \times n + m$. Of course, as discussed previously (1), relaxation matrices of the bound states can be expanded to include protons on the receptor as well as the ligand nuclei. Variations in the conformations of the ligands between free, binary and ternary complexes are described by the appropriate D_{ij} matrix, with dimensions $3(n + m) \times 3(n + m)$. In the above, we have changed the structure of this matrix relative to our previous treatment (1) by putting the terms for the uncomplexed ligands in the upper left hand corner, which simplifies the numbering of the matrix elements.

The kinetic matrix can be calculated based on a particular model for the formation of the ternary complex. A general description allowing either binary complex to form initially and to be converted into a ternary complex involves eight kinetic rate constants:



Consideration of the ligand equilibria reduces the number of independent rate constants to 7, e.g.,

$$k_{-4} = k_4 \left(\frac{k_1}{k_{-1}} \frac{k_{-2}}{k_2} \frac{k_{-3}}{k_3} \right). \quad [9]$$

A more specialized model requiring ordered binding of the two ligands is considered later. The analysis given below requires determination of the fractions of enzyme which are uncomplexed, involved in a binary complex with L_1 or L_2 , or in the ternary complex: pE , pEL_1 , pEL_2 , and pEL_1L_2 , respectively. These can be calculated at equilibrium using a King Altman analysis (9) and are given in the Appendix.

The kinetic matrix is then derived from the above kinetic scheme (e.g., 10). The diagonal terms correspond to the rates of disappearance of each species, L_1 , L_2 , EL_1 , EL_2 , and EL_1L_2 , with negative coefficients. The binary complexes EL_1 and EL_2 will disappear either due to dissociation, or to association of the second ligand. We then obtain a kinetic matrix of the form:

$$\mathbf{K} = \begin{array}{c} \begin{array}{cccccc} n & m & n & m & n & m \end{array} \\ \begin{array}{|c|c|c|c|c|c|} \hline (-k_1E & 0 & k_{-1}I & 0 & k_{-3}I & 0 \\ \hline -k_3EL_2I & (-k_2E & 0 & k_2I & 0 & k_{-4}I \\ \hline 0 & -k_4EL_1I) & 0 & k_2I & 0 & k_{-4}I \\ \hline k_1EI & 0 & (-k_{-1} & 0 & k_4I & 0 \\ \hline & & -k_4L_2)I & 0 & k_4I & 0 \\ \hline 0 & k_2EI & 0 & (-k_{-2} & 0 & k_{-3}I \\ \hline & & & -k_3L_1)I & 0 & k_{-3}I \\ \hline k_3EL_2I & 0 & k_4L_2I & 0 & (-k_{-3} & 0 \\ \hline & & & & -k_{-4})I & 0 \\ \hline 0 & k_4EL_1I & 0 & k_3L_1I & 0 & (-k_{-4} \\ \hline & & & & & -k_{-3})I \end{array} \end{array} \quad [10]$$

i.e., a system of block diagonal matrices (\mathbf{I} is the identity matrix with dimensions $n \times n$ or $m \times m$, as indicated) which interconvert individual spins between uncomplexed, binary complexed, and ternary complexed states, but lead to no other spin interconversions. Equation [1] is then generalized to the form:

$$\frac{d\mathbf{A}}{dt} = -(\mathbf{R}' + \mathbf{K})\mathbf{A}, \quad [11]$$

where \mathbf{R}' is the expanded relaxation matrix defined by Eq. [7], and \mathbf{K} the kinetic matrix given above.

The initial state of the \mathbf{A} matrix, $\mathbf{A}(0)$, is given by the diagonal matrix:

$$\mathbf{A}(0) = \begin{array}{c} \begin{array}{cccccc} n & m & n & m & n+m \end{array} \\ \begin{array}{|c|c|c|c|c|} \hline L_{1F}I & & & & \\ \hline & L_{2F}I & & & \\ \hline & & EL_1I & & \\ \hline & & & EL_2I & \\ \hline & & & & EL_1L_2I \\ \hline \end{array} \end{array} \quad [12]$$

where L_{1F} and L_{2F} are the free ligand concentrations, E , EL_1 , EL_2 , and EL_1L_2 are the concentrations of the free receptor, the two binary complexes and the ternary complex. In the above, $L_{1F} = L_1 - EL_1 - EL_1L_2$ and $L_{2F} = L_2 - EL_2 - EL_1L_2$ (see also Appendix A). Alternatively, it is convenient to introduce a normalized matrix $\mathbf{A}^N(0)$ which separately normalizes the contributions for the two ligands:

$$\mathbf{A}^N(0) = \begin{array}{|c|c|c|c|} \hline \frac{L_{1F}I}{L_1} & & & \\ \hline & \frac{L_{2F}I}{L_2} & & \\ \hline & & \frac{EL_1I}{L_1} & \\ \hline & & & \frac{EL_2I}{L_2} \\ \hline & & & & \frac{EL_1L_2I}{L_1} \\ \hline & & & & & \frac{EL_1L_2I}{L_2} \\ \hline \end{array} \quad [13]$$

Use of the above normalized matrix, $\mathbf{A}^N(0)$ leads to diagonal \mathbf{A} matrix terms which decay from 1 to 0, and is also consistent with linearization of the NOESY build-up curves discussed below.

Solution of Eq. [11] according to Eq. [6] leads to an NOE matrix of dimensions $3(n+m) \times 3(n+m)$, which describes all NOE interactions for a system which is in slow exchange. As discussed previously (1), transferred NOE interactions can in principle be observed under conditions of slow or fast exchange on the chemical shift time scale. Considering a single pair of spins—one on each ligand—there are in general 36 resonances in the 2D ILOE experiment described here, as illustrated in Fig. 1. In practice, resonances arising from the receptor complexes will be significantly broadened, making direct observation difficult. More generally, exchange on the chemical shift time scale will be sufficiently fast so that each group of nine resonances indicated by the squares in Fig. 1 will be exchange averaged. Under these conditions, it becomes useful to reduce the dimensionality of the NOESY \mathbf{A} matrix by defining a reduced “ \mathbf{C} ” matrix (1) according to

$$C_{ij} = A_{iF,jF} + A_{iF,jB} + A_{iF,jT} + A_{iB,jF} + A_{iB,jB} \\ + A_{iB,jT} + A_{iT,jF} + A_{iT,jB} + A_{iT,jT}, \quad [14]$$

where indices i and j denote the nuclei and subscripts F, B, and T refer to the free ligand, or to the binary or ternary complex. In terms of indices,

$$C_{ij} = A_{i,j} + A_{i+n+m,j} + A_{i,j+n+m} + A_{i+2(n+m),j} \\ + A_{i,j+2(n+m)} + A_{i+n+m,j+n+m} + A_{i+2(n+m),j+n+m} \\ + A_{i+n+m,j+2(n+m)} + A_{i+2(n+m),j+2(n+m)}. \quad [15]$$

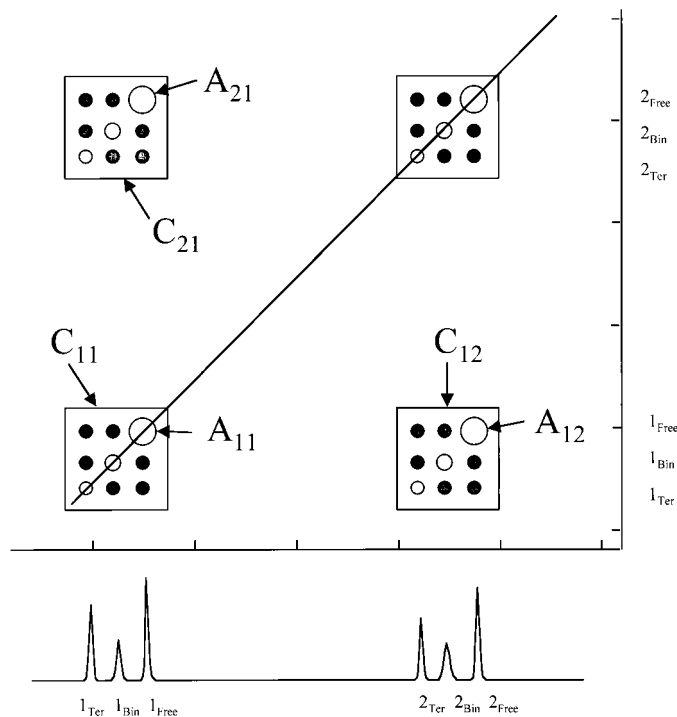


FIG. 1. Schematic representation of a 2D NOESY experiment for a system containing a pair of ligands, L_1 and L_2 , which can form binary or ternary complexes with a receptor E . The resonances arising from spin 1 are assumed to correspond to ligand 1, while those arising from spin 2 are assumed to correspond to ligand 2. The observation of separate resonances for each nucleus corresponding to the free, binary and ternary complexes would only be possible under conditions of slow chemical exchange. However, solution for all of the elements of the NOESY "A" matrix yields the time dependent NOE curves for each of these species. The dark cross peaks connecting resonances for a given spin are exchange peaks. The off diagonal open peaks are inter-nuclear NOEs. Although shown in this diagram, there would in general be no cross peaks connecting the nuclei of different ligands in the uncomplexed state or in the binary complexes in the absence of exchange. The remaining peaks are exchange-mediated NOE interactions. Under conditions of fast exchange, each group of nine matrix elements indicated by the squares can be summed to obtain the collapsed "C" matrix elements.

The C matrix has the same dimensionality as a relaxation matrix consisting of only the two ligands, i.e., $n + m \times n + m$. As in the case of the transferred NOE experiment treated previously, the dependence of the component A matrix elements corresponding to a given C matrix element on the mixing time can vary significantly. However, as the exchange rates become sufficiently high, each of the A matrix components corresponding to a given C matrix element exhibits the same limiting time dependence, with only differences in scaling factors among these elements. The C matrix cross peaks can also be normalized according to

$$C_{ij}^N = C_{ij} / (C_{ii} + C_{jj}) \quad [16]$$

using $A^N(0)$ in the calculation. This procedure extends the

linear range of the initial NOE build-up curves, facilitating the determination of the initial slope. Of course, more complex intermediate situations can exist in which the $L_1 \rightleftharpoons EL_1$ exchange is slow, the $L_2 \rightleftharpoons EL_2$ exchange intermediate, the $L_1 + EL_2 \rightleftharpoons EL_1L_2$ exchange slow, etc. Since the experiment is typically performed with a large excess of ligands over receptor, the first term in Eq. [14] will often be dominant, and the degree to which each of the component NOE contributions contributes will generally not be critical for the evaluation of the data.

NUMERICAL SIMULATIONS

As an illustration of the above approach, we consider a system of two ligands, each containing three spins in a linear arrangement separated by 2.5 Å. In the ternary complex, the ligands form a linear array of six spins, each with the same 2.5 Å separation (Fig. 2). Simulations have been performed by modifying the previously described TRNOE program written in *Mathematica* (1) as outlined by the theoretical treatment given above. For the simulations shown in Fig. 3, we have assumed that there is neither positive nor negative cooperativity of binding, so that $k_1 = k_3$ and $k_{-1} = k_{-3}$ and similarly, $k_2 = k_4$ and $k_{-2} = k_{-4}$. Thus, ligand 1 associates and dissociates with the same rate constant regardless of whether ligand 2 is present, and vice versa. We have set the association rate constants equal to $10^8 \text{ M}^{-1} \text{ s}^{-1} = 10^5 \text{ mM}^{-1} \text{ s}^{-1}$, and the dissociation rate constants to 10^3 s^{-1} , which corresponds to equilibrium dissociation constants of $10 \text{ } \mu\text{M}$. In our experience, this value for the association rate constant reasonably approximates diffusion controlled ligand binding for a variety of systems (1, 11–13). For these values, the receptor will exist primarily in the ternary complex form at millimolar ligand concentrations typically used for such studies. The NOESY cross peak intensities corresponding to the free ligand only,

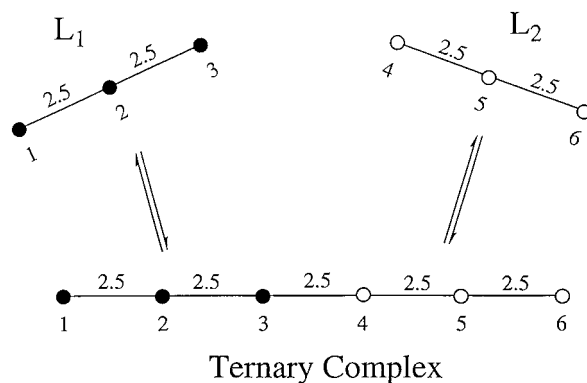


FIG. 2. Schematic representation of an exchanging system of two ligands, L_1 and L_2 , each having three spins in a linear arrangement separated by 2.5 Å each. In the ternary complex, the two ligands form a linear array of six spins, with all distances equal to 2.5 Å, i.e., the distance between spins 3 and 4 is equal to each of the intra-ligand spin separations. For simplicity, the two binary complexes are not shown.

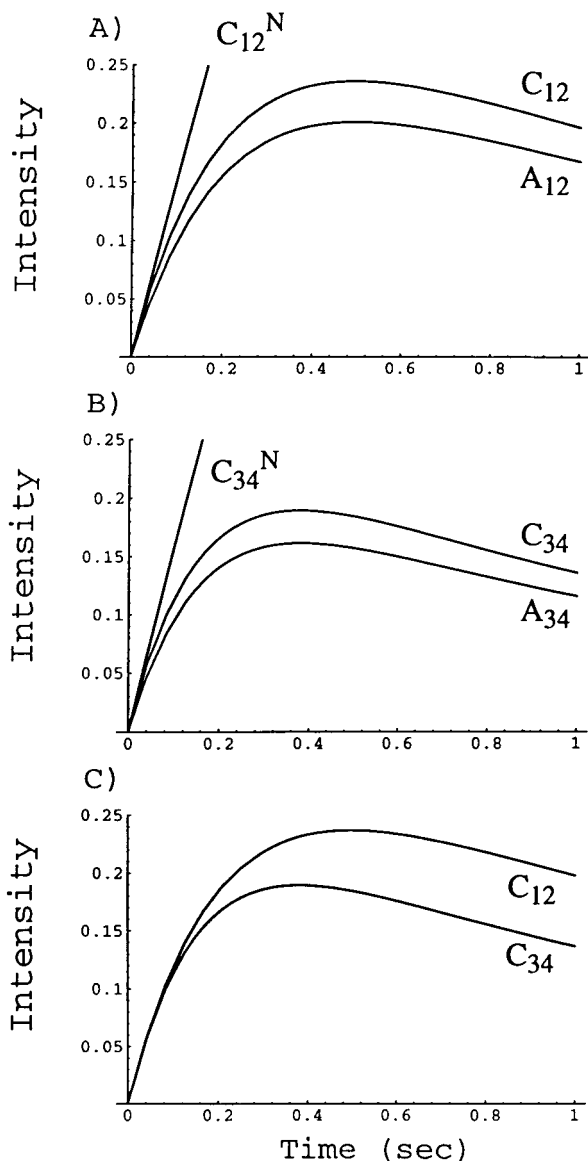


FIG. 3. Intensities of NOE resonances for the system shown in Fig. 2. (A) Time dependence of the usual, intra-ligand TRNOE cross peaks connecting spins 1 and 2: A_{12} and C_{12} , where, as discussed in the text, the former corresponds to the free species only, and the latter to all of the nine elements connecting spins 1 and 2. Also shown is the normalized matrix element, C_{12}^N , calculated as described by Eq. [16], which is approximately linear for short times. (B) The corresponding calculations for A_{34} , C_{34} , and C_{34}^N . (C) A comparison of the intraligand TRNOE curve C_{12} and the interligand ILOE curve C_{34} . For these parameters, the similarity in the initial slopes mirrors the similar r_{12} and r_{34} distances in the bound state. Other parameters are: $\nu = 500$ MHz, $\tau_{1F} = \tau_{2F} = 10^{-10}$ s, $\tau_B = 10^{-7}$ s, $[L_1] = [L_2] = 5$ mM; $[E_0] = 0.4$ mM; $k_1 = k_2 = k_3 = k_4 = 10^8 \text{ M}^{-1} \text{ s}^{-1} = 10^5 \text{ mM}^{-1} \text{ s}^{-1}$; $k_{-1} = k_{-2} = k_{-3} = k_{-4} = 10^3 \text{ s}^{-1}$. Based on these concentrations and rate constants, we obtain $pE = 4 \times 10^{-6}$; $pEL_1 = pEL_2 = 2 \times 10^{-3}$; and $pEL_1L_2 = 0.996$ As in our previous calculations (1), a leakage relaxation rate, $\rho^* = 1 \text{ s}^{-1}$, is included in the relaxation matrix for each of the bound nuclei.

i.e., assuming that chemical exchange among all species is slow on the NMR time scale, and the cross peak intensities derived from the “C” matrix, i.e., assuming fast exchange for

a given nucleus between free, binary, and ternary complexes are shown in Fig. 3. Other parameters used for the simulation are: $\nu = 500$ MHz, $[L_1] = [L_2] = 5$ mM, $[E] = 0.4$ mM, $\tau_{1F} = \tau_{2F} = 10^{-10}$ s and $\tau_B = 10^{-7}$ s, where τ_{1F} and τ_{2F} correspond to free ligands 1 and 2, and τ_B to the binary or ternary complexes. Also shown in Fig. 3 is the linearized initial slope, C_{ij}^N , defined above, which at short mixing times approximates a straight line tangential to the initial slope of C_{ij} .

As in the case of the time-dependent TRNOE curves, the presence of the free species acts to extend the time scale of the NOE curve, so that development of the ILOE peaks for the exchanging ligands is more gradual than for the bound species. For the parameters given above, the exchange is sufficiently rapid so that the results obtained using the **C** matrix are qualitatively almost identical to those obtained using the dominant **A** matrix term for the free ligand, and only slightly greater in magnitude, e.g., compare A_{12} and C_{12} . Thus, the NOE information of the complex is effectively transferred to, and stored by, the uncomplexed ligand. Of primary significance is the fact that the calculated NOE between nuclei 3 and 4 on different ligands (C_{34}) builds up with essentially the same initial rate as the calculated NOE between nuclei 1 and 2 (C_{12}). Thus, to the extent that the above set of assumptions holds, internuclear distances between ligands can be calculated on the basis of known internuclear distances within either ligand. However, as discussed below, a number of the assumptions used here may not generally apply, so that care must be exercised in the quantitative interpretation of ILOE data. Alternatively, the conditions which must be met in order to determine relative inter-ligand distances are less demanding. The most significant issue from this standpoint is the need to correctly account for indirect relaxation effects, e.g., by modeling the dependence of the various ILOE and TRNOE cross peaks on mixing time.

In view of the similarity between the inter and intraligand NOE build-up curves, it can be anticipated that ILOE curves will show similar indirect relaxation effects. The A_{13} and C_{13} curves are compared with the A_{24} and C_{24} curves in Fig. 4. All parameters are identical with those used for the calculation in Fig. 3. Thus, the inter-ligand NOE curve for nonadjacent spins exhibits the same apparent lag as the intra-ligand curve. As expected, a comparison with the simulations in Fig. 3 indicates that the magnitudes of the C_{13} and C_{24} interactions are substantially reduced relative to the curves for C_{12} or C_{34} . The simulations in Fig. 4 show the typical lag in the build-up curves which is predicted for TRNOE cross peaks corresponding to indirectly dipolar-coupled nuclei, as long as the exchange rates are sufficiently high (1).

Effects of slower exchange rates were modeled by keeping the association rate constants and other parameters as in Fig. 3, while reducing the dissociation rate constants by two orders of magnitude. Under such conditions the exchange process becomes too slow to effectively transfer the NOE information to the uncomplexed ligands. This leads to markedly nonlinear

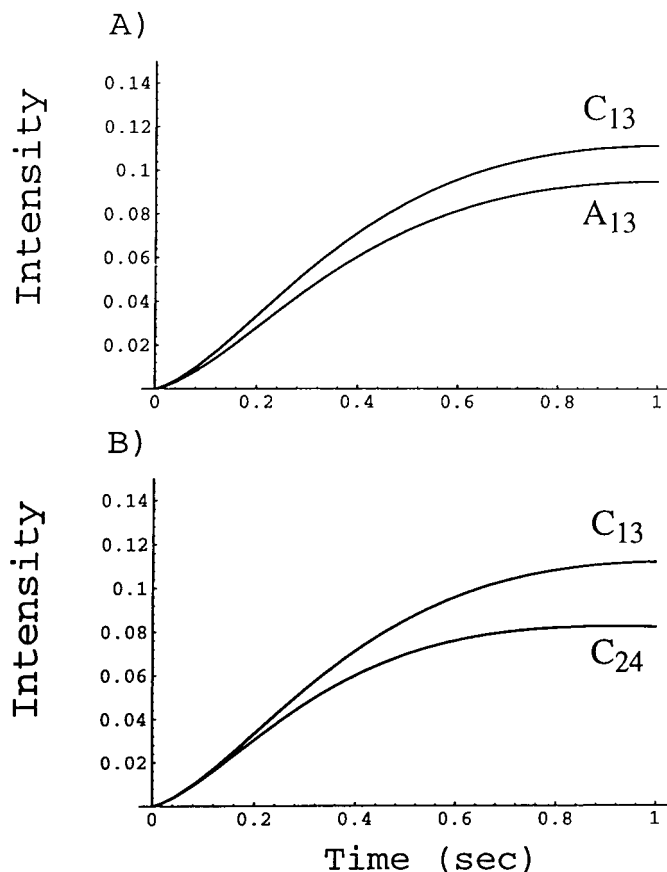


FIG. 4. Time-dependence of NOESY cross peaks corresponding to (A) the nuclei 1 and 3 on ligand 1, and (B) a comparison of the C_{13} and C_{24} curves connecting nuclei on different ligands. All curves are characterized by the apparent lag which characterizes contributions due to the indirect relaxation pathways: $1 \leftrightarrow 2 \leftrightarrow 3$ for C_{13} , and $2 \leftrightarrow 3 \leftrightarrow 4$ for C_{24} . We also note the difference in magnitudes of the effect relative to the calculations for adjacent nuclei (Fig. 3). All simulation parameters are identical with those used in Fig. 3.

behavior of the initial portion of the NOE curves, as illustrated in Fig. 5 calculated with all dissociation rate constants set to 10 s^{-1} (Fig. 5), and to a general reduction in magnitude of the effect. The A_{ij} and C_{ij} curves no longer exhibit a similar time dependence, although they tend to be nearly parallel for most of the simulation period. The initial negative values for A_{12} arise due to the contribution from the free ligand. In fact, for the correlation time $\tau_F = 10^{-10} \text{ s}$ used in the simulations, the entire A_{12} curve is negative in the absence of exchange. In contrast, A_{34} does not go negative for any exchange rates, since there is no contribution to this element from the uncomplexed ligands. (We note again that the convention used here is that negative corresponds to anti-diagonal, but to positive NOE values.) Unexpectedly, there is a cross over of the NOE curves so that $C_{34} > C_{12}$ toward the end of the simulation period. This behavior appears to arise because the two terminal nuclei 3 and 4 relax somewhat more slowly than nucleus 2 which has two

neighboring spins 2.5 \AA away, leading to a more rapid decay of A_{12} or C_{12} as compared with A_{34} or C_{34} .

Alternatively, an increase in the dissociation rate constants for ligand 2 by two orders of magnitude relative to the values used for the simulation shown in Fig. 3 has only a minor effect on the ILOE C_{34} and C_{56} elements (Fig. 6). A further increase in $k_{-2} = k_{-4}$ to 10^6 s^{-1} significantly reduces the fraction of enzyme in the ternary complex, giving $pEL_1 = 0.665$ and $pEL_1L_2 = 0.333$. This is associated with a significant decrease in both C_{56} and C_{34} relative to C_{12} . Increasing the dissociation rate constants to 10^7 s^{-1} corresponds to $pEL_1 = 0.95$ and $pEL_1L_2 = 0.048$, and eliminates most of the interligand NOE. An interesting effect in this case is that C_{34} is somewhat greater than C_{56} , the intra-ligand NOE for ligand 2. As discussed in greater detail below, this appears to arise from a negative NOE contribution from the uncomplexed ligand under some conditions, which can occur for transferred NOE peaks but not for ILOE peaks. The simulation shown in Fig. 6C illustrates that distances derived from ILOE resonances can be compared to intra-ligand distances derived from TRNOE resonances even if

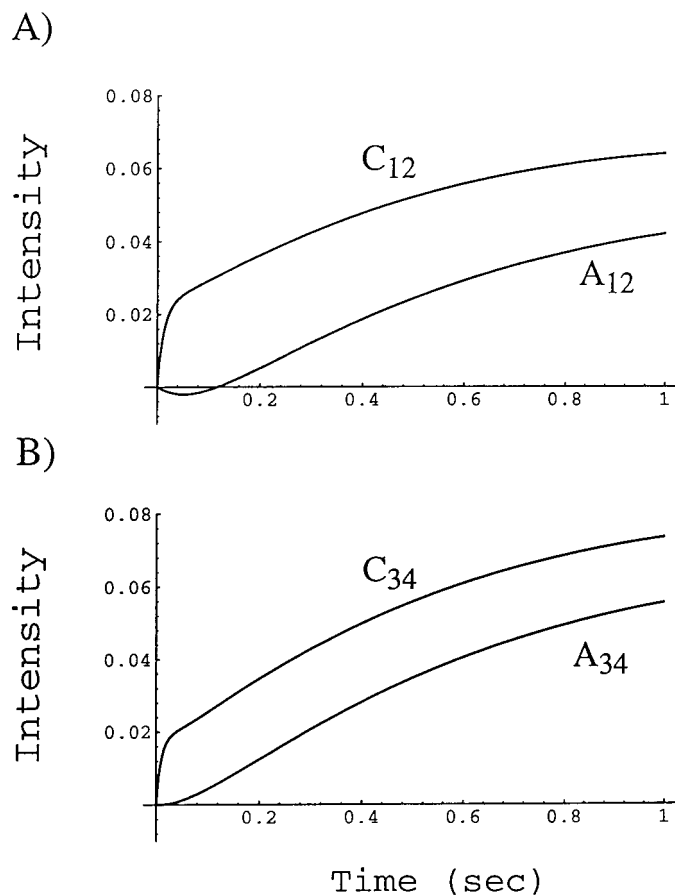


FIG. 5. Effects of slower exchange on the time-dependent TRNOE (A) and ILOE (B) cross peak intensities. The geometry is as described in Fig. 2, and the parameters as listed in Fig. 3, with the exception that $k_{-1} = k_{-2} = k_{-3} = k_{-4} = 10 \text{ s}^{-1}$. For these parameters, nearly all of the receptor remains in the complexed state, $pEL_1L_2 = 0.99996$.

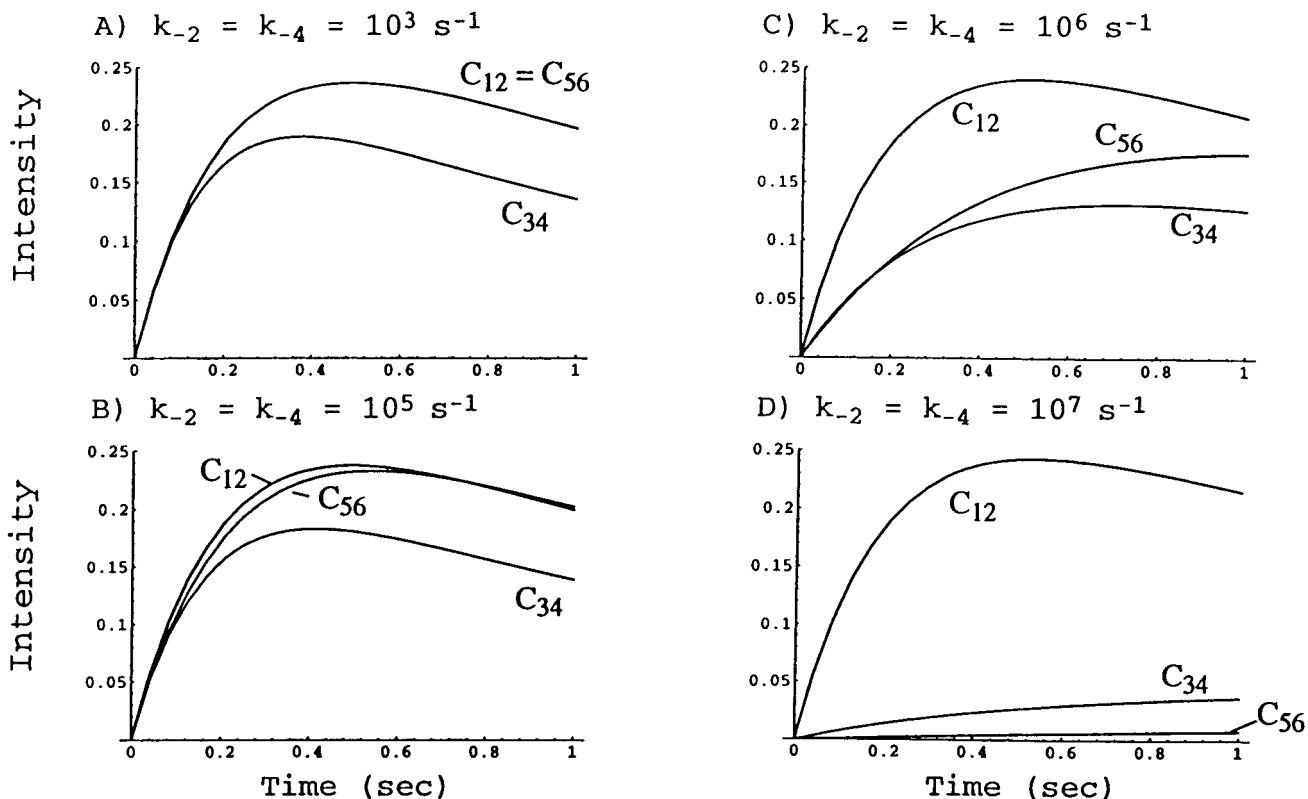


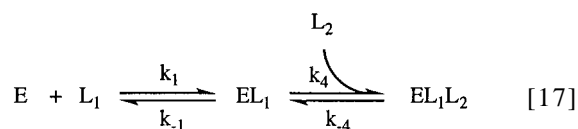
FIG. 6. Effects of greater dissociation rates for ligand L_2 on TRNOE and ILOE cross peaks. This figure shows the C_{12} , C_{56} , and C_{34} NOE curves corresponding to $k_{-2} = k_{-4} =$ (A) 10^3 s^{-1} , (B) 10^5 s^{-1} , (C) 10^6 s^{-1} , and (D) 10^7 s^{-1} . All other parameters as in Fig. 3. For these parameters, most of the receptor exists either as the binary complex with L_1 or as the ternary complex; the corresponding fractional populations are: (A): $p_{EL_1} = 0.0008$, $p_{EL_1L_2} = 0.996$, (B): $p_{EL_1} = .166$, $p_{EL_1L_2} = 0.832$, (C): $p_{EL_1} = .665$, $p_{EL_1L_2} = 0.333$, (D): $p_{EL_1} = 0.95$, $p_{EL_1L_2} = 0.048$.

the receptor is not saturated, by comparing the build-up rates for inter-ligand cross peaks with those in ligand 2, due to the similar fractions of receptor complex involved. In general, however, intensity comparisons between ILOE and TRNOE peaks require independently determined kinetic information as well as a considerable amount of caution.

One of the major differences between TRNOE and ILOE studies apparent from recent experimental work (2) is the magnitude of the inter-ligand inter-nuclear distances relative to typical intraligand distances. Thus, a typical ligand may have many internuclear distances of $\sim 1.8 \text{ \AA}$ for methylene protons, or 2.5 \AA for vicinal aromatic protons, while internuclear distances arising from even the closest pair of protons on distinct ligands are generally not less than 3 \AA and of course, can be much greater. Then, due to the $1/r^6$ dependence of the build-up rate, it becomes necessary to use significantly longer mixing periods. The basic geometry of Fig. 2 has been modified so that the intra-ligand distances are 3.5 \AA and the inter-ligand distances 2.5 \AA (Fig. 7A) or vice versa (Fig. 7B). For the first geometry, the ILOE peaks develop more rapidly than the TRNOE peaks, while the reverse is obtained for the geometry used for the simulations shown in Fig. 7B. The geometry used for the Fig. 7A calculation is expected to be less typical, while

the geometry used for the calculation shown in Fig. 7B is probably more typical of experimental systems likely to be encountered. One interesting aspect of the ILOE curves illustrated by a comparison of Figs. 7A and 3B is that the reduction in the intra-ligand relaxation which results from the greater internuclear distances results in a substantially greater maximum for the ILOE peak. Hence, all other factors being equal, ligands with less favorable intra-ligand relaxation interactions are more likely to exhibit ILOE peaks. Nevertheless, recent experimental studies involving NADPH indicate that significant ILOE peaks can be observed even for the pyridine CH_2 protons (2).

Since many enzymes enforce ordered ligand binding, simulations were also performed using the kinetic model shown below:



where we have used k_1/k_{-1} and k_4/k_{-4} to facilitate comparison

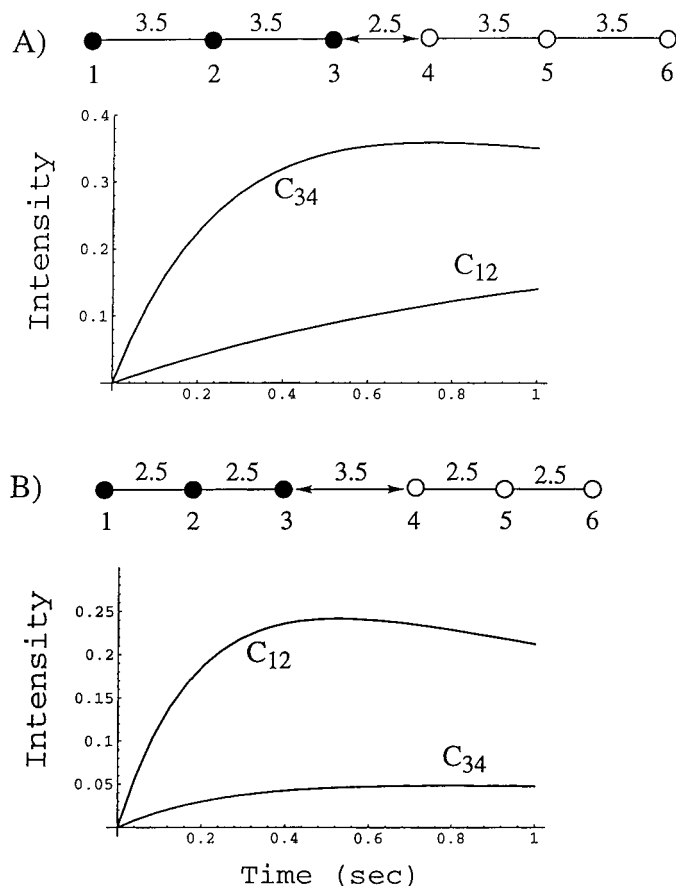


FIG. 7. Effects of geometric variations on TRNOE and ILOE curves. Relative to above simulations based on the geometry shown in Fig. 2, the intra-ligand distances have been increased to 3.5 Å for the calculation shown in (A), and the inter-ligand distances increased to 3.5 Å for the calculation shown in (B). Other parameters are as in Fig. 3.

with the model of Eq. [8]. According to the kinetic scheme shown above, L_2 can bind only after L_1 , and L_1 can dissociate only from the binary (EL_1) complex. Although the equations involved in determining the ratio of the different species are considerably simpler than those corresponding to the kinetic scheme shown in Eq. [8], (Appendix A), the calculated TRNOE and ILOE curves are more complex. This arises because the ordered binding model introduces a fundamental asymmetry into the problem which is absent from the random order binding model of Eq. [8]. This is illustrated by the simulation shown in Fig. 8A, which corresponds to the same geometry shown in Fig. 2 and to the same parameter values used for the simulations of Fig. 3. In this case, the predicted TRNOE curve for C_{56} (or A_{56}) is very similar to that shown in Fig. 3A for C_{12} (or A_{12}), while the TRNOE curves for ligand 1 and the ILOE curves differ dramatically. The appearance of A_{12} or C_{12} is indicative of much slower exchange kinetics for ligand 1. Thus, the A_{12} and C_{12} curves do not exhibit the same qualitative time dependence, with C_{12} appearing as approximately a superposition of an initial positive region correspond-

ing to the NOE for the binary and ternary complexes, plus a slower negative contribution from the free species. Increasing k_{-1} to 10^4 s^{-1} (Fig. 8B) leads to more effective NOE transfer, although the initial portion of the C_{12} curve remains markedly nonlinear. Interestingly, a set of nearly identical curves is obtained using $k_{-1} = 10^3 \text{ s}^{-1}$ and $k_{-4} = 10^4 \text{ s}^{-1}$. Further increase of both k_{-1} and k_{-4} to 10^4 s^{-1} leads to much more effective transfer of the intra- and interligand NOEs (Fig. 8C). Increasing $k_{-1} = k_{-4}$ to 10^6 s^{-1} reverses the trend. For these parameters, the fractional occupation of the receptor by ligand 1 is greater than that by ligand 2, $pEL_1 > pEL_1L_2$. Since for these dissociation rate constants, binding is too weak to produce strong transferred NOE or ILOE values, the effect of the ordered binding constraint in slowing down the apparent exchange rate for ligand 1 leads to more effective transfer of nuclear polarization for this ligand.

For several of the simulations of Fig. 8, as well as Fig. 6D, the ILOE cross peak intensity is greater than some of the TRNOE intensities for pairs of nuclei at the same internuclear distance. This phenomenon appears to occur in situations in which a negative contribution arising from the intra-ligand NOE of the uncomplexed species reduces the transferred NOE due to slow exchange conditions and/or to poor binding of the ligand to the receptor. The NOE is thus reduced by contributions from the uncomplexed ligand. This effect is not present when the ligand binds well and the exchange is sufficiently rapid to lead to a strong transfer of the bound NOE. No corresponding effect can occur for the inter-ligand Overhauser effect, since there is no interaction between the nuclei in the uncomplexed pair of ligands.

DISCUSSION

Transferred nuclear Overhauser effect studies have proven to be a useful approach for the analysis of the conformation of flexible ligands complexed with receptors (1, 14–20). In general, inter-ligand Overhauser effects as described here appear not to have been observed previously. This most probably results from the fact that most, although not all (21–25) transferred NOE studies utilize only a single receptor ligand, or do not use sufficiently long mixing times which are generally required to observe ILOE cross peaks. Two related observations have appeared in the literature involving the NAD-glutamate dehydrogenase complex (24) and albumin-lactate-water (25), but in both cases, the interpretation of the data as arising from inter-ligand Overhauser effects is equivocal. In the glutamate dehydrogenase-NAD complex, proximity of NAD molecules bound at the active and regulatory sites was inferred from long range transferred NOE interactions, for example between nicotinamide ribose protons N1' and N3'; however, spin diffusion in the large complex (glutamate dehydrogenase is a hexamer with MW = 332,000) (26) could also explain these observations. Consistent with this interpretation, recent crystallographic studies of this enzyme show an allosteric

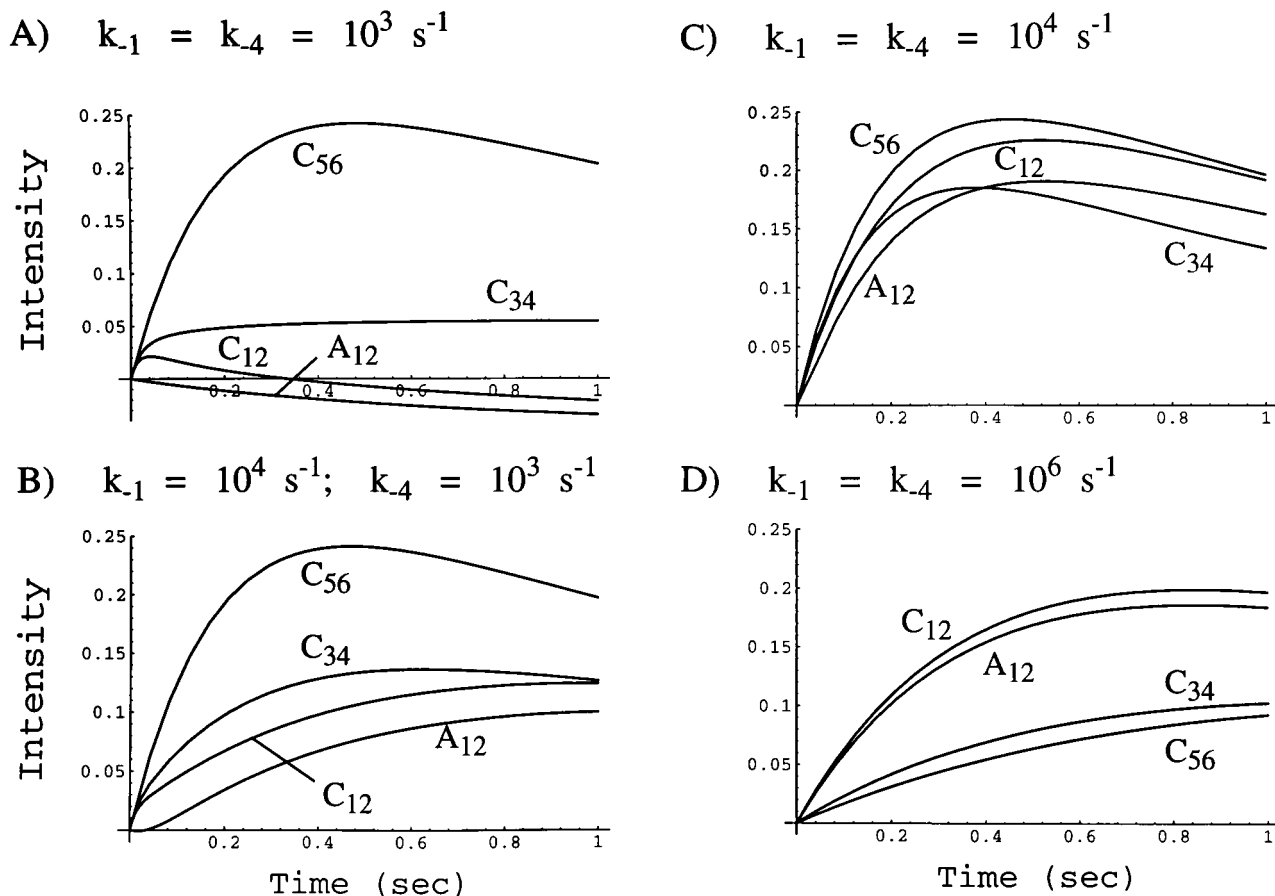


FIG. 8. Simulations of an ordered binding kinetic model (Eq. [17], Appendix) for the geometric model shown in Fig. 2. For all simulations, $k_1 = k_4 = 10^5 \text{ mM}^{-1} \text{ s}^{-1}$, and other parameters are as in Fig. 3. (A) $k_{-1} = k_{-4} = 10^3 \text{ s}^{-1}$ (calculated $pE = 4.72 \times 10^{-6}$; $pEL_1 = 2.17 \times 10^{-3}$; $pEL_1L_2 = 0.998$); (B) $k_{-1} = 10^4 \text{ s}^{-1}$; $k_{-4} = 10^3 \text{ s}^{-1}$ (calculated $pE = 4.72 \times 10^{-5}$; $pEL_1 = 2.17 \times 10^{-3}$; $pEL_1L_2 = 0.998$); (C) $k_{-1} = k_{-4} = 10^4 \text{ s}^{-1}$ (calculated $pE = 4.62 \times 10^{-4}$; $pEL_1 = 2.13 \times 10^{-2}$; $pEL_1L_2 = 0.978$); (D) $k_{-1} = k_{-4} = 10^6 \text{ s}^{-1}$ (calculated $pE = 0.598$; $pEL_1 = 0.275$; $pEL_1L_2 = 0.127$), and $pEL_2 = 0$ in all cases. Interestingly, using parameters: $k_{-1} = 10^3 \text{ s}^{-1}$; $k_{-4} = 10^4 \text{ s}^{-1}$ resulted in curves which were nearly identical to those of simulation (B) above, but correspond to different calculated fractional species concentrations: (calculated $pE = 4.63 \times 10^{-5}$; $pEL_1 = 2.13 \times 10^{-2}$; $pEL_1L_2 = 0.979$).

NADH binding site which is $\sim 20 \text{ \AA}$ from the active site (27). For the case of NOEs observed between water and lactate in the presence of 20% (w/w) cross-linked bovine serum albumin, several possible interpretations were considered (25), and the effect of the viscosity of the concentrated protein solution on the water/lactate relaxation may also be significant.

Recent experimental studies involving several dehydrogenases (2) provide unequivocal confirmation of the existence of such effects, and suggest that for initial evaluation of ILOEs, it is optimal to use relatively long mixing times, $\sim 700 \text{ ms}$. This condition arises since typically the distances between nuclei on different ligands will be larger than many of the intra-ligand distances, and the dipolar interaction is a sensitive function of this distance. A more complete study involving the use of a set of mixing times is then valuable for separating indirect and direct relaxation pathways. These data can be modeled using the formalism developed here. However, comparison of TRNOE and ILOE peak intensities to derive relative distances is difficult, and requires independent evaluation of the kinetic

parameters. In general, the cross peak intensities in a NOESY experiment can be viewed as falling into two regimes: the initial NOE build-up regime and a subsequent relaxation regime during which the effect dies away. It can be anticipated that in practice, optimal mixing times for ILOE observations will often fall into the first category, at which many of the TRNOE peaks will be well into the relaxation phase. Although quantitation of inter-ligand distances will generally be difficult and subject to a number of constraints, information on relative internuclear distances is more readily derived from these measurements and can provide useful information on relative ligand orientation (2).

In view of the general similarities predicted for the behavior of ILOE and TRNOE resonances, effects of protein spins previously considered in the context of TRNOE studies (1), and currently under evaluation in terms of ILOE studies, are likely to be qualitatively similar. Calculations performed by making the leakage term ρ_B^* much larger than 1 s^{-1} show that the NOE effects are drained off by the protein so that the

maximum in the TRNOE and ILOE curves is reduced, although the basic shapes of the curves remain similar. As another limiting case, we have considered a geometry in which the binary complex with ligand 2 is characterized by very short internuclear distances. The effects in this case depend on the fractions of pEL_2 and pEL_1L_2 which are present. As pEL_2 increases, the TRNOE effects for L_2 show more rapid build-up and decay, while the ILOE effects are reduced. Protein-mediated spin diffusion can in general be minimized through the use of NOESY experiments which suppress spin-diffusion (28, 29), or eliminated via protein deuteration (30). Analogous inter-ligand ROE experiments may also prove useful for dealing with spin diffusion (31). Deuteration not only minimizes potentially misleading protein-mediated interactions, but also lengthens the bound ligand T_1 values, enhancing the "magnetic memory" of the ligand for interactions in the receptor complex. Thus, Shibata *et al.* (30) report observation of weak TRNOE cross peaks between ligand protons greater than 4 Å apart in TRNOE studies using perdeuterated phosphoglycerate kinase.

In addition to deuteration of the protein, deuteration strategies that increase the ligand T_1 values, e.g., deuteration of alternate sites, can also produce significant improvements in the observation of both TRNOE (31) and ILOE resonances. The effect of ligand T_1 is illustrated by a comparison of the simulations for C_{34} between Fig. 3B and Fig. 7A, as noted above. The calculated curves correspond to the same kinetic and NMR parameters, but to different geometries, having the same 3–4 inter-ligand distance in the ternary complex, but greater intra-ligand distances for the simulation of Fig. 7A. The resulting reduction of the intra-residue relaxation rates for the latter geometry results in an increased length of the period during which the ILOE is increasing, and to an increased maximum effect, from ~ 0.19 (at $t_m = 0.38$ s) to 0.36 (at $t_m = 0.75$ s). Hence, strategies which lengthen the relaxation rates for the ligand protons, e.g., specific deuteration (31), can facilitate observation of inter-ligand Overhauser effects.

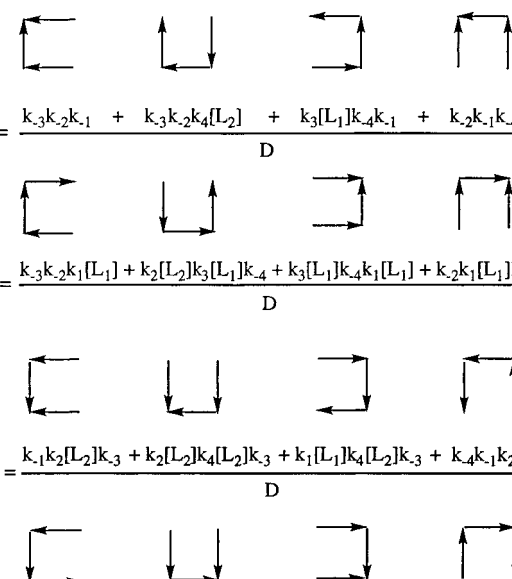
The observation of ILOE interactions between spins on different ligands should prove to be a valuable tool for understanding active site geometry, hence providing insight into active site chemistry. It also seems reasonable to anticipate that ILOE's can be used in a complementary fashion with other inhibitor-discovery approaches such as the SAR by NMR technique (22, 32) in order to design enzyme inhibitors from component ligands. In this type of application, contributions from indirect, protein-mediated relaxation pathways may prove useful for the identification of ligands which are bound too far away from one another to exhibit significant direct ILOEs.

APPENDIX A

Calculation of Equilibrium Receptor–Ligand Fractional Populations

For the kinetic model of Eq. [8], the equilibrium fractions of E, EL_1 , EL_2 , and EL_1L_2 can be determined from a King–

Altman analysis (9) according to the diagrams illustrated below. Each term must be divided by the denominator, D , equal to the sum of all 16 terms for normalization.



$$pE = \frac{E}{E_0} = \frac{k_{-3}k_2k_{-1} + k_{-3}k_2k_4[L_2] + k_3[L_1]k_4k_{-1} + k_2k_1k_4}{D}$$

$$pEL_1 = \frac{EL_1}{E_0} = \frac{k_{-3}k_2k_1[L_1] + k_2[L_2]k_3[L_1]k_4 + k_3[L_1]k_4k_1[L_1] + k_2k_1[L_1]k_4}{D}$$

$$pEL_2 = \frac{EL_2}{E_0} = \frac{k_1k_2[L_2]k_3 + k_2[L_2]k_4[L_2]k_3 + k_1[L_1]k_4[L_2]k_3 + k_4k_1k_2[L_2]}{D}$$

$$pEL_1L_2 = \frac{EL_1L_2}{E_0} = \frac{k_1k_2[L_2]k_3[L_1] + k_2k_3[L_1]k_4[L_2]^2 + k_3k_4[L_2]k_1[L_1]^2 + k_2k_1[L_1]k_4[L_2]}{D}$$

For the case of ordered ligand binding described by Eq. [17], the fractional populations are given by

$$pE = \frac{E}{E_0} = \frac{k_{-1}k_{-4}}{k_{-1}k_{-4} + k_1[L_1]k_{-4} + k_1[L_1]k_4[L_2]}$$

$$pEL_1 = \frac{EL_1}{E_0} = \frac{k_1[L_1]k_{-4}}{k_{-1}k_{-4} + k_1[L_1]k_{-4} + k_1[L_1]k_4[L_2]}$$

$$pEL_2 = \frac{EL_2}{E_0} \equiv 0$$

$$pEL_1L_2 = \frac{EL_1L_2}{E_0} = \frac{k_1[L_1]k_4[L_2]}{k_{-1}k_{-4} + k_1[L_1]k_{-4} + k_1[L_1]k_4[L_2]}$$

The above equations are dependent on the free ligand concentrations: $[L_1] = L_{1F}$ and $[L_2] = L_{2F}$, which in the limit $L_1, L_2 \gg E_0$ can be replaced by the total ligand concentrations, $L_{1F} = L_1$ and $L_{2F} = L_2$. Since under conditions that allow observation of ILOE peaks the enzyme is often effectively saturated with both ligands, a more accurate result is obtained by setting $L_{1F} = L_1 - E_0$ and $L_{2F} = L_2 - E_0$. One manifestation of the error resulting from these approximations is the calculated asymmetry, $(A_{ij} - A_{ji})/A_{ij}$ or $(C_{ij} - C_{ji})/C_{ij}$. For the parameters given in Fig. 3, the calculated asymmetry can be several percent in some cases, but is reduced to $\sim 10^{-9}$ or less using the above approximation.

ACKNOWLEDGMENTS

Several helpful suggestions from Dr. Dawei Li and Dr. Eugene DeRose are gratefully appreciated. A copy of the ILOE *Mathematica* program used for the simulations will be deposited on the NIEHS NMR group web site at <http://dir.niehs.nih.gov/dirlsb/nmrhome.htm>, after it has been sufficiently annotated.

REFERENCES

1. R. E. London, M. E. Perlman, and D. G. Davis, Relaxation matrix analysis of the transferred nuclear Overhauser effect for finite exchange rates, *J. Magn. Reson.* **97**, 79–98 (1992).
2. D. Li, E. DeRose, and R. E. London, The inter-ligand Overhauser effect: A powerful new NMR approach for mapping structural relationships of macromolecular ligands, *J. Biomol. NMR* **15**, 71–76 (1999).
3. S. Macura and R. R. Ernst, Elucidation of cross relaxation in liquids by two-dimensional N.M.R. spectroscopy, *Mol. Phys.* **41**, 95–117 (1980).
4. J. T. Gerig, Transient Fluorine-Proton Overhauser Effects in (4-Trifluoromethyl)benzenesulfonyl-a-chymotrypsin, *J. Am. Chem. Soc.* **102**, 7308–7312 (1980).
5. J. W. Keepers and T. L. James, A theoretical study of the distance determinations from NMR. Two-dimensional nuclear Overhauser effect spectra, *J. Magn. Reson.* **57**, 404–426 (1984).
6. T. M. G. Koning, R. Boelens, and R. Kaptein, Calculation of the nuclear Overhauser effect and the determination of proton-proton distances in the presence of internal motions, *J. Magn. Reson.* **90**, 11–123 (1990).
7. Ishima, S. Shibata, and K. Akasaka, General features of proton longitudinal relaxation in proteins in solution, *J. Magn. Reson.* **91**, 455–465 (1991).
8. N. Khan, A. Graslund, A. Ehrenberg, and J. Shriver, Sequence-specific ¹H NMR assignments and secondary structure of porcine motilin, *Biochemistry* **29**, 5743–5751 (1990).
9. I. H. Segel, "Enzyme Kinetics," pp. 506–523, Wiley, New York (1975).
10. J. Jeener, B. H. Meier, P. Bachmann, and R. R. Ernst, Investigation of exchange processes by two-dimensional NMR spectroscopy, *J. Chem. Phys.* **71**, 4546–4553 (1979).
11. A. M. Gronenborn and G. M. Clore, *Biochemistry* **21**, 4040 (1982); M. E. Davis, J. D. Madura, J. Sines, B. A. Luty, S. A. Allison, and J. A. McCammon, Diffusion-controlled enzymatic reactions, *Methods Enzymol.* **202**, 473–497 (1991).
12. J. Eyschen, B. Vitoux, S. Rahuel-Clermont, M. Marraud, G. Brantlant, and M. T. Cung, Phosphorus-31 nuclear magnetic resonance studies on coenzyme binding and specificity in glyceraldehyde-3-phosphate dehydrogenase, *Biochemistry* **35**, 6064–6072 (1996).
13. D. G. Davis, M. E. Perlman, and R. E. London, Direct measurement of the dissociation rate constant for inhibitor-enzyme complexes via the T_{1ρ} and T₂ (CPMG) methods, *J. Magn. Reson. B* **104**, 266–275 (1994).
14. J. P. Albrand, B. Birdsall, J. Feeney, G. C. K. Roberts, and A. S. V. Burgen, The use of transferred nuclear Overhauser effects in the study of the conformations of small molecules bound to proteins, *Int. J. Biolog. Macromol.* **1**, 37–41 (1979).
15. F. Ni, Recent developments in transferred NOE methods, *Prog. NMR Spectrosc.* **26**, 517–606 (1994).
16. A. M. Gronenborn and G. M. Clore, Determination of ligand conformation in macromolecular complexes using the transferred nuclear Overhauser effect, *Biochem. Pharmacol.* **40**, 115–119 (1990).
17. H. N. B. Moseley, E. V. Curto, and N. R. Krishna, Complete relaxation and conformational exchange matrix (CORCEMA) analysis of NOESY spectra of interacting systems—2-Dimensional transferred NOESY, *J. Magn. Reson. B* **108**, 243–261 (1995).
18. G. M. Lippens, C. Cerf, and K. Hallenga, Theory and experimental results of transfer-NOE experiments. 1. The influence of the off rate versus cross-relaxation rates, *J. Magn. Reson.* **99**, 268–281 (1992).
19. N. R. Nirmala, G. M. Lippens, and K. Hallenga, Theory and experimental results of transfer NOE experiments. II. The influence of residual mobility and relaxation centers inside the protein on the size of transfer NOEs, *J. Magn. Reson.* **100**, 25–42 (1992).
20. A. P. Campbell and B. D. Sykes, Theoretical evaluation of the 2-dimensional transferred nuclear Overhauser effect, *J. Magn. Reson.* **93**, 77–92 (1991).
21. B. Meyer, T. Weimar, and T. Peters, Screening mixtures for biological activity by NMR, *Eur. J. Biochem.* **246**, 705–709 (1997).
22. P. J. Hajduk, E. T. Olejniczak, and S. W. Fesik, One-dimensional relaxation- and diffusion-edited NMR methods for screening compounds that bind to macromolecules, *J. Am. Chem. Soc.* **119**, 12,257–12,261 (1997).
23. J. Czaplicki and A. Milon, Simulations of transferred NOE in a ternary peptide-receptor-lipid complex, *J. Chim. Phys.* **95**, 196–207 (1998).
24. A. Banerjee, H. R. Levy, G. C. Levy, C. LiMuti, B. M. Goldstein, and J. E. Bell, A transfer nuclear Overhauser effect study of coenzyme binding to distinct sites in binary and ternary complexes in glutamate dehydrogenase, *Biochemistry* **26**, 8443–8450 (1987).
25. S. D. Swanson, Protein mediated magnetic coupling between lactate and water protons, *J. Magn. Reson.* **135**, 248–255 (1998).
26. E. L. Smith, B. M. Austen, K. M. Blumenthal, and J. F. Nyc, Glutamate dehydrogenases, In "The Enzymes" (P. D. Boyer, Ed.), Vol. 11, pp. 293–367, Academic Press, New York.
27. P. E. Peterson and T. J. Smith, The structure of bovine glutamate dehydrogenase provides insights into the mechanism of allostery, *Structure* **7**, 769–782 (1999).
28. J. Fejzo, W. M. Westler, J. L. Markley, and S. Macura, Complete elimination of spin diffusion from selected resonances in two-dimensional cross-relaxation spectra of macromolecules by a novel pulse sequence, *J. Am. Chem. Soc.* **114**, 1523–1524 (1992).
29. S. J. F. Vincent, C. Zwahlen, C. B. Post, J. W. Burgner, and G. Bodenhausen, The conformation of NAD⁺ bound to lactate dehydrogenase determined by nuclear magnetic resonance with suppression of spin diffusion, *Proc. Natl. Acad. Sci. U.S.A.* **94**, 4383–4388 (1997).
30. C. G. Shibata, J. D. Gregory, B. S. Gerhardt, and E. H. Serpersu. Kinetic, binding, and NMR studies of perdeuterated yeast phosphoglycerate kinase and its interactions with substrates, *Arch. Biochem. Biophys.* **319**, 204–210 (1995).
31. M. E. Perlman, D. G. Davis, G. W. Koszalka, J. V. Tuttle, and R. E. London, Studies of inhibitor binding to Escherichia coli purine nucleoside phosphorylase using the transferred nuclear Overhauser effect and rotating-frame nuclear Overhauser enhancement, *Biochemistry* **33**, 7547–7559 (1994).
32. S. B. Shuker, P. J. Hajduk, R. P. Meadows, and S. W. Fesik, Discovering high affinity ligands for proteins: SAR by NMR, *Science* **274**, 1531–1534 (1996).